

Substrate-mediated ordering and defect analysis of a surface covalent organic frameworkOualid Ourdjini, Rémy Pawlak, Mathieu Abel,^{*} Sylvain Clair,[†] Liang Chen, Nathalie Bergeon, Michel Sassi, Vincent Oison, Jean-Marc Debierre, Roland Coratger,[‡] and Louis Porte[§]*Aix-Marseille Univ, IM2NP, CNRS UMR6242, Faculté des Sciences et Techniques, Campus de Saint Jérôme, Case 142, 13397 Marseille Cedex 20, France*

(Received 17 March 2011; revised manuscript received 27 May 2011; published 9 September 2011)

We investigate the growth of a two-dimensional polymer obtained by dehydration of 1,4-benzenediboronic acid (BDBA). The molecules are vapor deposited under ultrahigh vacuum conditions on well-oriented noble metal—Ag(111), Ag(100), Au(111), and Cu(111)—surfaces. Molecular flux and substrate temperature are varied to obtain a polymer of optimum quality, whose structure best approaches that of an ideal honeycomb network. We find that a high molecular flux (~ 0.1 monolayer/minute) is necessary to initiate BDBA polymerization on all surfaces at room temperature. Once polymerization has extensively taken place, the robust surface network can resist a temperature of 450 °C. However, various kinds of defects are present within this two-dimensional surface polymer. Statistical analyses, primarily based on the minimal spanning tree approach, are performed to quantify polymer order. They indicate that Ag(111) and Ag(100) surfaces are better templates than Au(111) surfaces for polymer formation, far more than Cu(111) ones. The influence of the metal nature on the polymer growth is discussed with respect to the surface diffusion of adsorbed molecules.

DOI: [10.1103/PhysRevB.84.125421](https://doi.org/10.1103/PhysRevB.84.125421)

PACS number(s): 68.37.Ef, 82.35.-x, 81.16.Dn, 05.70.Np

I. INTRODUCTION

In the last decade, supramolecular self-assembly at surfaces has proven to be very efficient for creating atomically controlled organic nanostructures.^{1,2} The noncovalent character of intermolecular interactions, ranging from Van der Waals interactions to hydrogen or metal-organic bonds, is highly flexible and provides reversibility and defect self-healing that is required to produce perfectly ordered and well-extended superstructures. However, the low stability of such networks and the lack of electronic communication between the molecules prevent practical applications in harsh environments. In this regard, the possibility of extending the concepts of supramolecular chemistry to the formation of covalent bonds between molecular tectons has attracted recent attention.^{3,4} While two-dimensional (2D) polymers are expected to have great impact on many fundamental and applied aspects of science, the search for synthetic routes leading to reliable and robust periodic covalent molecular sheets is still in its infancy.⁵ Some recent demonstrations of covalent polymerization performed directly at surfaces have opened promising perspectives.^{6–36} In all these systems, however, the growth control is very delicate, and the polymers formed are either restricted to one-dimensional growth or poorly ordered or limited in terms of 2D extension. An in-depth understanding of the complex mechanisms governing on-surface polymerization is still needed before such systems can be practically controlled and used.

Boronic acids can undergo a self-condensation (dehydration) reaction to give rigid boroxine rings and planar polymer sheets.³⁷ The process of dehydration leading to the formation of an ideal honeycomb-like polymer is recalled Fig. 1. By using 1,4-benzenediboronic acid (BDBA) evaporated onto a well-defined metal surface under ultrahigh vacuum conditions, we could grow extended nanoporous 2D networks.¹⁶ An important advantage of this approach is that it allows easy tuning of the structure of as-formed networks.³⁸ However, several kinds of defects were inherently formed, and the polymer structure

always deviated from an ideal honeycomb two-dimensional network. We thus decided to explore the different growth parameters (evaporation flux, substrate nature, and temperature) to determine the experimental conditions that would reduce all kinds of defects and produce optimum growth conditions for an ideal honeycomb network. An important issue then was to generate relevant parameters that could properly quantify the structural quality of the polymer. We performed statistical analyses of our scanning tunneling microscopy (STM) images to quantify the advancement of the polymerization process and could assess the polymer quality as a function of the experimental growth conditions.

II. EXPERIMENTS AND RESULTS

BDBA molecules were vapor deposited in ultrahigh vacuum conditions on noble metal surfaces, Ag(111), Ag(100), Au(111), and Cu(111), from a graphite crucible. Molecular depositions was investigated in the submonolayer regime, from very low to near complete monolayer coverage, and characterized using scanning tunneling microscopy (STM) and low-energy electron diffraction (LEED) in a separate chamber connected to the evaporation chamber. During molecule evaporation, the chamber vacuum was maintained below 10^{-9} mbar. Various combinations of source (T_c) and substrate (T_s) temperatures were used to determine which growth parameters favor the polymerization of BDBA molecules. The crucible temperature was varied between 90 and 110 °C, thus allowing change in the molecular deposition rate from about 0.005 ML/min for $T_c = 90$ °C to 0.1 ML/min for $T_c = 110$ °C. A series of experiments were done using different temperature combinations between crucible temperature and substrate temperature, $[T_c-T_s]$. Unless otherwise stated, the results presented here were obtained using the following parameter sets: $[T_c = 90$ °C, $T_s = \text{RT}]$, $[T_c = 110$ °C, $T_s = \text{RT}]$, $[T_c = 110$ °C, $T_s = 150\text{--}250$ °C], which are experimental conditions making it possible to seize the main characteristics of, and some remarkable differences in, the molecular growth

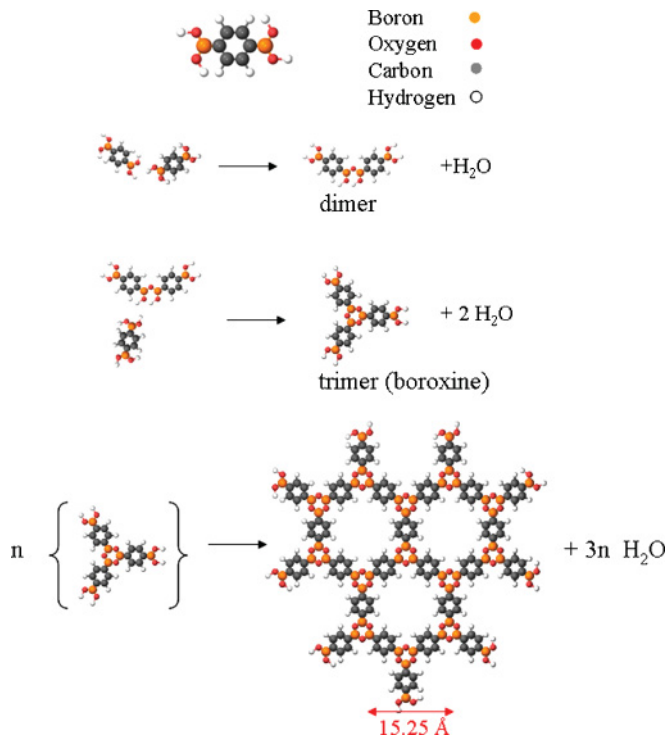


FIG. 1. (Color online) BDBA molecule dehydration reaction scheme leading to the ideal 2D polymer framework.

on the four metal surfaces. Here, $T_c = 90^\circ\text{C}$ and $T_c = 110^\circ\text{C}$ determined the hereafter called low and high molecular fluxes, respectively. Room temperature (RT) was $\approx 20^\circ\text{C}$. All STM experiments were performed at RT.

Figure 2(a) shows a STM image recorded after BDBA deposition on Cu(111) at low flux [$T_c = 90^\circ\text{C}$, $T_s = \text{RT}$]. Small molecular aggregates of circular shape were imaged. They diffused slowly overnight to form larger islands of undefined shape. Annealing the sample at 100°C led to the formation of BDBA trimers attributed to boroxine entities that are key structures for polymer growth (Fig. 1). However, extended polymer formation was not observed at that stage [Fig. 2(b)]. Increasing the annealing temperature did not significantly change the molecular arrangement, and finally the degradation of the layer was obtained at about 300°C . By comparison, the polymerized BDBA layer obtained on Ag(111) actually degraded first after annealing at a temperature beyond 450°C .¹⁶ Figure 2(c) shows an STM image of deposition on Cu(111) at RT using an increased molecular flux [$T_c = 110^\circ\text{C}$, $T_s = \text{RT}$]. Finally, Fig. 2(d) shows an STM image of the organic layer obtained after deposition at high flux temperature and high substrate temperature [$T_c = 110^\circ\text{C}$, $T_s = 150^\circ\text{C}$]. These images (insets) give clear evidence of connections between trimers giving a branched construction and the eventual formation of closed cells resulting from some advanced polymerization process. Obviously, increasing T_s from RT to 150°C provides better polymerization and better surface covering, as expected from an increased diffusion of molecules on the surface. However, it is worth noting that polymerization can occur even on a substrate maintained at RT, provided that the molecular flux is sufficiently high. Indeed, the first polymerization steps are visible at high flux [$T_c = 110^\circ\text{C}$, $T_s = \text{RT}$] [Fig. 2(c)] but not

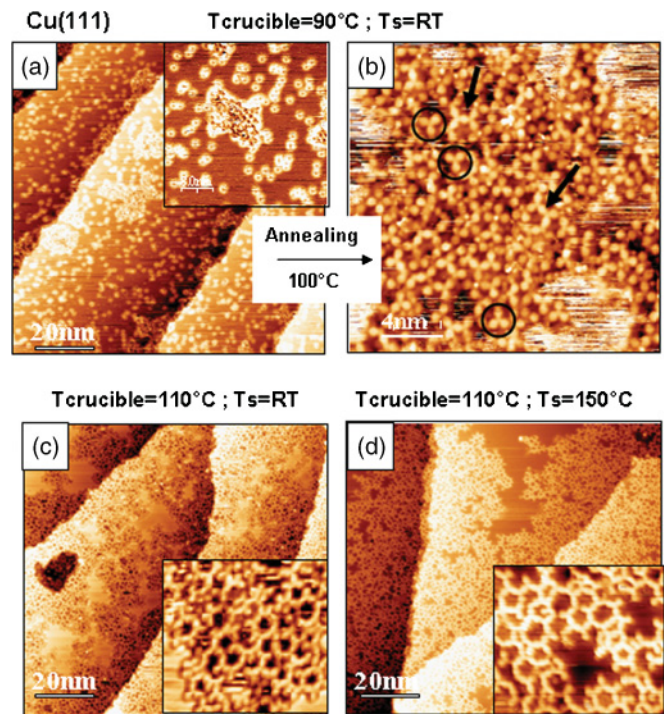


FIG. 2. (Color online) (a) STM image of BDBA molecules deposited at low flux on a Cu(111) surface at room temperature. (b) Same surface after annealing at 100°C . Boroxine-based trimers were obtained, three of which are emphasized by circles. Also shown by arrows, two patterns resulting from the linking between a trimer and a dimer (see Table I). (c) STM image of BDBA molecules deposited on a Cu(111) surface at high flux ($T_c = 110^\circ\text{C}$, $T_s = \text{RT}$). The first polymerisation steps occur. (d) STM image of BDBA molecules deposited on a Cu(111) surface ($T_c = 110^\circ\text{C}$, $T_s = 150^\circ\text{C}$). The polymer extends on the surface.

at low flux [$T_c = 90^\circ\text{C}$, $T_s = \text{RT}$] [Fig. 2(a)]. Thus, besides the substrate temperature, the molecular flux is another key parameter for the advancement of the polymerization process.

Figures 3(a)–(c) summarize the results obtained after deposition of BDBA molecules on Au(111). Using a low molecular flux ($T_c = 90^\circ\text{C}$) and a substrate kept at RT, it was possible to obtain nearly complete surface covering [Fig. 3(a)]. Molecules here self-assemble mainly into a periodic superlattice with a rectangular unit cell ($a = 0.5 \pm 0.05 \text{ nm}$, $b = 1.0 \pm 0.05 \text{ nm}$). This structure is identical to that obtained when BDBA molecules are deposited on a KCl substrate, and similar to the lamellar structure of the bulk crystal.³⁹ Pawlak *et al.*⁴⁰ showed that strong hydrogen bonds are responsible for the cohesion of this phase. Heating the surface led to the desorption of the complete molecular layer, except for the few molecules that polymerized at step edges [Fig. 3(b)] and that were then stable even after annealing at near 400°C . Using the experimental conditions [$T_c = 110^\circ\text{C}$, $T_s = 110^\circ\text{C}$], providing high molecular flux and high surface mobility, the molecular layer appeared radically different [Fig. 3(c)]. Molecules here reacted on the surface and formed various disordered oligomers and patches of hexagonal rings, yet of limited extension.

Deposition on an Ag(111) surface at RT and at low molecular flux ($T_c = 90^\circ\text{C}$) produced an H-bonded supramolecular

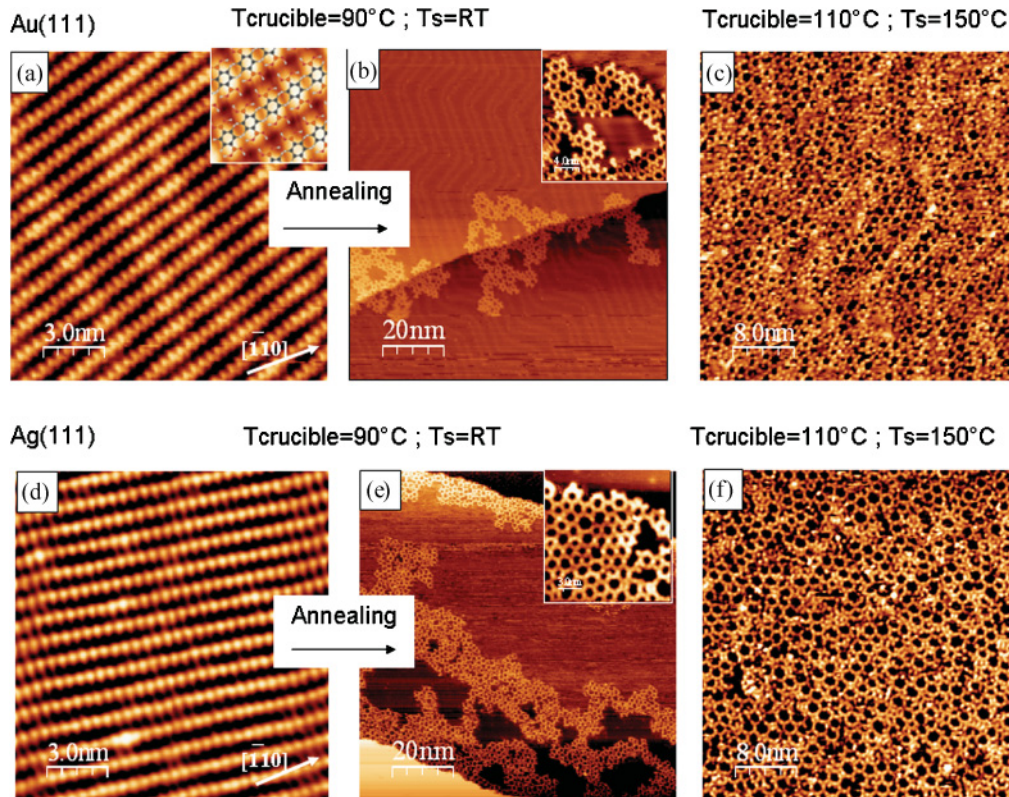


FIG. 3. (Color online) (a) STM images of BDBA molecules deposited on an Au(111) surface at low flux, $T_c = 90^\circ\text{C}$, $T_s = \text{RT}$ showing the H-bonded supramolecular phase. (b) Same deposition after heating at 350°C ; most of the molecules have desorbed except near step edges where polymerization occurred. (c) STM images of BDBA molecules deposited on an Au(111) surface at high flux ($T_c = 110^\circ\text{C}$, $T_s = 150^\circ\text{C}$). The polymer extends on the surface. (d) STM image of BDBA molecules deposited on an Ag(111) surface at low flux ($T_c = 90^\circ\text{C}$, $T_s = \text{RT}$) showing the presence of an H-bonded supramolecular phase. (e) Same deposition after heating at 350°C . (f) BDBA polymerization obtained on Ag(111) at high flux ($T_c = 110^\circ\text{C}$, $T_s = 150^\circ\text{C}$). The extended polymer phase degrades upon heating beyond 450°C .

phase, a polymer phase, and a molecular gas phase [Fig. 3(d)]. The rectangular unit cell of the H-bonded phase was similar to that obtained on Au(111). On Ag(111), the polymer phase also anchored to step edges, and annealing at $250\text{--}350^\circ\text{C}$ led to an extension of the surface covered by the polymer phase [Fig. 3(e)]. Increasing both T_c to 110°C and T_s to 150°C led to a wide covering of the surface by a dense polymer phase, composed essentially of hexagon units [Fig. 3(f)]. This polymer phase could be heated up to 450°C before degradation begins.

Finally, doing the same experiments on Ag(100) surface indicated a great likeness with Ag(111). The only noticeable difference was that the H-bonded supramolecular phase self-assembled more easily on Ag(100) than on Ag(111). Indeed, depositions at either low or high flux on Ag(100) at RT led to the formation of the H-bonded phase.

III. DISCUSSION

A. An imperfect polymerization process

1. Kinds of defects

Following the dehydration process, BDBA molecules polymerize, ideally to form a honeycomb two-dimensional network. In solution, polymer sheets stack to grow a lamellar solid.^{37,38} When BDBA molecules are deposited on noble

metal surfaces, polymerization can be obtained similarly. Hexagonal pores, the unit cells involved in the formation on the ideal honeycomb network, are observed. Besides these ideal hexagon units, the molecular layer exhibits defects such as pentagons, heptagons, and other defects of variable shapes. It is, however, worth noting that, like hexagon units, pentagon (or heptagon) units can be obtained after complete dehydration, giving closed polygons, 5 (or 7) BDBA molecules being linked covalently. Pentagons and heptagons can be obtained, thanks to a very small angle distortion of the phenyl-boroxine molecular bonds (Fig. 4). Enthalpies of formation have been calculated for the three polygon units using density functional theory (DFT) and the SIESTA package.^{41–43} They amount to rather close values: 0.508, 0.554, and 0.535 eV per molecule for hexagon, pentagon, and heptagon, respectively. It is otherwise known that the boron-oxygen bond is labile; small differences in the bond lengths and angles are observed in most oxoboron molecules.⁴⁴ It thus appears as a general feature that boroxine rings represent flexible linkages that can withstand some strain energy. This is the reason why nonhexagonal polygon patterns can actually form.⁴⁵ This is in particular true for pentagons and heptagons which both contribute to the covalent polymer phase. Pentagon-heptagon pair defects are similarly found in graphene.⁴⁶ Other kinds of defects arise when the polygons have not been closed, most probably due to volume hindrance between molecules when the packing density increases. The

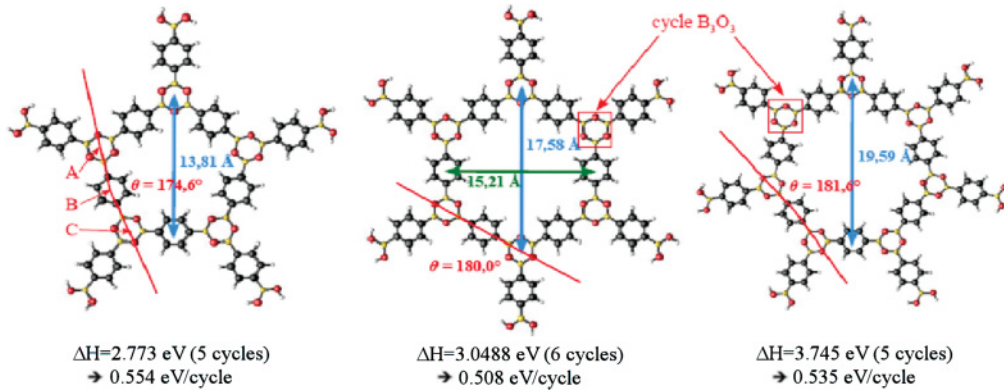


FIG. 4. (Color online) Pentagon, hexagon, and heptagon pore structures obtained by DFT simulations.

dehydration process is thus incomplete. Post annealing at increased temperature to reduce these defects is not efficient, even up to 450 °C, the temperature beyond which the polymer network begins to degrade. It means that strong bonds, iono-covalent in nature, link all molecular units together, thus inhibiting any significant reorganization after the framework has formed. All kinds of defects induce distortion of the polymer network and possible stress in the 2D molecular layer.

2. Statistical analysis

Although strong intermolecular bonds form between BDBA molecules, surface-molecule interactions cannot be entirely ignored. Our results show that the polymerization process is directly influenced by the underlying metal. The polymer network that was obtained on the noble metal surfaces can be regarded as a defective network grown on an ideal honeycomb basis, and more simply as a disordered hexagonal pattern. This situation presents some analogy with the Bénard–Marangoni instability appearing in convective experiments: while a regular pattern of hexagons represents the most stable structure, topological defects that are mainly pentagon-heptagon pairs and aggregates of irregular polygons are observed.⁴⁷ A major issue in the study of such complex systems is to find out suitable methods for their analysis.

There are several ways to quantify disorder in patterns. The easiest and most obvious one is to count the defects. The ratio of the number of defects to the total number of cells is one major measure of disorder. A defect here is defined as a boronic acid group that has not reacted and represents a local ending of the polymer growth. In our STM images, we carefully counted the number of molecules having reacted to form boron-oxygen bonds. It was thus possible to define the degree of reaction advancement $\tau_R = N/4M$, where N is the number of boron-oxygen bonds that formed following the dehydration reaction, and M is the number of molecules involved. Hence $\tau_R = 1.0$ for an ideal infinite hexagonal network (Fig. 1). Table I reports some theoretical values of τ_R calculated for molecular assemblies likely to occur in the first steps of the polymerization process. Table II reports experimental τ_R values derived from statistical analyses on several STM images (averaged over several thousands of molecules) for polymer grown on the Cu, Au, and Ag surfaces. This gives an accurate quantification of the ability of the different surfaces to conduct

the reaction between BDBA molecules. The degree of reaction advancement on the Cu surface ($\tau_R = 0.60$) is distinctly lower than on the Au ($\tau_R = 0.76$) and Ag surfaces ($\tau_R = 0.79$). It is also lower than the one calculated for ideal hexagonal units ($\tau_R = 0.66$), which means that the polymerization process of BDBA molecules on Cu(111) is restricted to its very first stage (Fig. 2). This limited degree of polymerization explains the lower thermal stability of BDBA layers formed on Cu(111), by comparison with the layers formed on the other two surfaces.

Even though this global parameter gives a good measure of the polymerization reaction advancement, it fails to take into account other defects, such as stress-induced pattern distortions, pentagons, or heptagons, which are ignored because they are built from reacted molecules. Also, it does not take into account the global morphology of the polymer and the formation of extended pores, which inherently appear even for the best quality polymer shown in Fig. 3. There are several methods of topographical analysis of spatial point patterns, and the most commonly used were tested by Wallet and Dussert.⁴⁸ They demonstrated that multiparameter methods are really more discriminating than monoparameter ones. According to their analysis, the method which gives the smallest standard error for one distribution and a good distribution power and stability has been recognized to be based on the minimal spanning tree (MST) edge length distribution graph. This method allows the characterization and quantification of the order hidden behind the disorder in any distribution of points on a surface. It was first introduced by Dussert *et al.*⁴⁹ to study disorder in sets of lithium aggregate particles grown on a dielectric substrate. It was thereafter successfully used to carry

TABLE I. Degree of reaction advancement τ_R defined as the number N of B-O bonds formed after dehydration, divided by the initial number of hydroxyl groups : $\tau_R = N/4M$ (M : number of molecules involved) calculated for the most probable initial steps occurring during the polymerization process.

N	M	τ_R
2	2	0.25
6	3	0.50
12	5	0.60
24	9	0.66
28	10	0.70

TABLE II. Degree of reaction advancement τ_R obtained by counting reacted and nonreacted molecules on the four metal surfaces (average from several STM images and thousands of molecules).

Metal surface	τ_R
Cu(111)	0.60
Au(111)	0.76
Ag(100)	0.79
Ag(111)	0.79

out the statistical analysis of the disorder of two-dimensional cellular arrays in directional solidification.^{50,51} The MST approach was also demonstrated to be a sound method for the study of disorder in 2D Bénard–Marangoni convective patterns.⁵² Therefore, the MST method is meaningful to quantify the order-disorder level of our patterns. Considering a distribution of points on a surface, the MST is a graph without any closed loop that connects all the points of the distribution and for which the sum of the edge lengths (point-to-point distances) is minimum. For a specific pattern, an MST construction is not unique, but all possible MSTs are equivalent so that the histogram of the edge lengths is unique. In our case, the points used to construct the MST were defined by the center of mass of cells built by molecules. Raw STM images were first processed to clearly delineate the borders of cells. Then some specific analysis procedures developed with Visilog-Noesis software were run to determine the position of the center of mass and the surface of each cell, and finally to build the MST. The MST starts from any cell center, and its length is increased by successive connections to the closest neighboring center. Figure 5 shows an example of such construction. The histogram of edge lengths used to build the MST was then computed to extract the average edge length m^* and the corresponding standard deviation σ^* . These quantities were normalized following Eq. (1) so that the distribution can be plotted in a (m, σ) diagram and compared to any other 2D arrangement:

$$m = \frac{m^*}{\sqrt{\langle S \rangle}} \frac{(N-1)}{N} \quad \text{and} \quad \sigma = \frac{\sigma^*}{\sqrt{\langle S \rangle}} \frac{(N-1)}{N}, \quad (1)$$

where $\langle S \rangle$ is the average area of cells and N the number of cells used for the MST construction. Billia *et al.*⁵⁰ demonstrated that at least 200 cells should be considered to obtain the convergence of m and σ values.

Particular arrangements called mosaics, for which $\sigma = 0$, are composed of an infinite set of regular polygons. The null value of standard deviation characterizes obviously periodic networks, whereas the m value depends on the periodic lattice. For simple mosaics obtained with hexagons or squares, m values are 1.075 and 1, respectively. These models have been reported on the (m, σ) graph in Fig. 6. Dussert *et al.*⁴⁹ progressively randomized regular mosaics by giving each point a new position deduced from its previous one using a Gaussian distribution of increasing standard deviation. The trajectory joining the perfect hexagon mosaics point ($m = 1.075, \sigma = 0$) and the random arrangement point ($m = 0.662, \sigma = 0.311$) allows the evaluation of the degree of disorder introduced in the initial hexagonal network. When the disorder

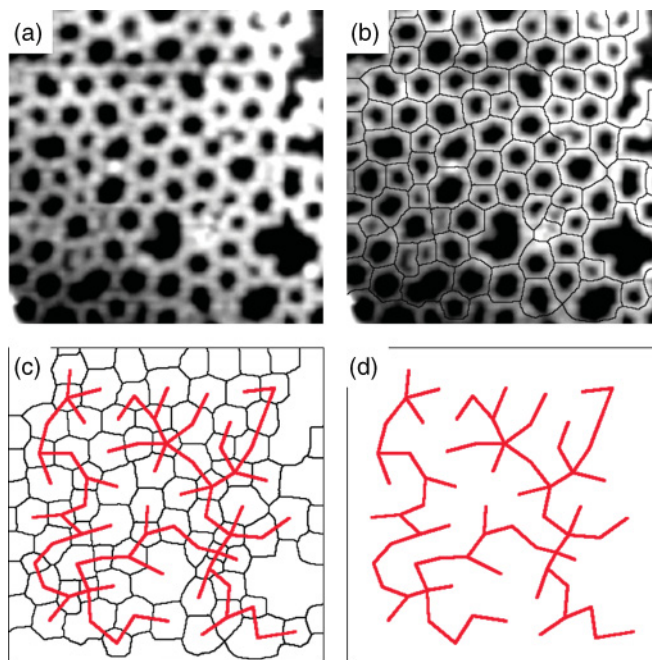


FIG. 5. (Color online) Minimal spanning tree (MST) construction for an STM image of a BDBA polymer. (a) Raw STM image. (b) Skeletonized STM image. (c) Skeleton superimposed with the minimal spanning tree. (d) Minimal spanning tree.

becomes high, the geometry of the underlying pattern becomes undistinguishable, and the two curves joining the random distribution to the hexagonal and square patterns converge for $\sigma > 0.2$.

The (m, σ) values obtained from several images of the four metal surfaces investigated (the number of cells was in the range 200–1,000, depending on images) were determined.

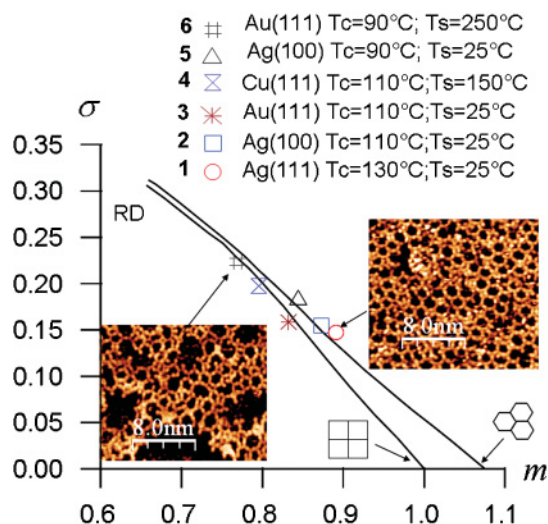


FIG. 6. (Color online) The (m, σ) diagram. Here, m and σ values derived from the MST method are reported for BDBA layers deposited on Ag, Au, and Cu surfaces. All deposits were annealed at 200–300 °C, except triangular point. The relative position of points along the path between the perfect hexagon mosaics and the random arrangement (RD) reflects the quality of the BDBA polymerization. STM images show characteristic arrangements from extreme points.

They are reported in Fig. 6. The vicinity of the measured points to the line joining the random distribution to the perfect hexagonal tiling confirms in all cases the hexagonal nature of the polymer pattern.

Let us first consider points 1, 2, 3, and 4 deduced from STM images recorded after evaporation of BDBA molecules on Ag(111), Ag(100), Au(111), and Cu(111), respectively, under experimental conditions for optimal polymer growth (i.e. high molecular flux, $T_c = 110$ °C; sample temperature T_s between RT and 150 °C; postannealing temperature in the range 200–300 °C). The graph unambiguously demonstrates that the Cu(111) surface produces more disorder in the polymer than the silver and gold surfaces do. Ag(111) and Ag(100) surfaces behave very similarly and are characterized by a polymer formation closest to an ideal hexagonal pattern. Au(111) represents an intermediate case.

We also reported point six, which corresponds to a deposition on Au(111) at low flux ($T_c = 90$ °C) and high temperature aiming at increasing the possibility of collisions between molecules. Clearly this was not efficient and point six corresponds to a high degree of disorder, as illustrated by the inserted STM image. From point six to point three, the molecular flux was increased by a factor of more than 10, which again emphasizes the crucial importance of the flux in polymer formation.

We mentioned above that the main difference between Ag(111) and Ag(100) was an H-bonded phase that preferably formed on the latter. Starting from this phase on Ag(100), it was possible to observe slow polymer formation within a timeframe of several tens of hours, the molecular layer being kept at room temperature. The polymer finally obtained in such conditions corresponds to point five and exhibits less order than the polymer corresponding to point two that was also performed on Ag(100) but under experimental conditions preventing the formation of a H-bonded phase.

The MST approach thus appears as an efficient tool to quantify the quality of the polymer that forms on the different metal surfaces. However, the (m, σ) graph, which measures the deviation from perfect hexagonal tiling, does not inform about the kind of defects involved. In particular, the formation of pentagons and heptagons introduces deviation from hexagonal tiling in the (m, σ) graph. Nevertheless, these defects results from covalent bonding (Fig. 4) and thus fully participate in the polymerization process.

As already mentioned, the procedure developed with Visilog-Noesis allows the determination of cell areas, i.e. areas of the pores in the present case. Figure 7 gives the six histograms corresponding to the six points drawn in the (m, σ) graph (Fig. 6). The theoretical areas corresponding to pentagons, hexagons, and heptagons are 1.35, 2.0, and 2.8 nm², respectively. Experimentally, for one geometric structure (five- or six- or seven-sided cells), the pores may undergo some distortion, and small variations in size measurements may also be generated by the skeletonization process applied to raw images. Thus, size measurements do not give thin and separated peaks centered on theoretical values but a much more continuous distribution. The width of the histogram bars was then defined as the theoretical difference between hexagon and pentagon areas to clearly distinguish between different geometries.

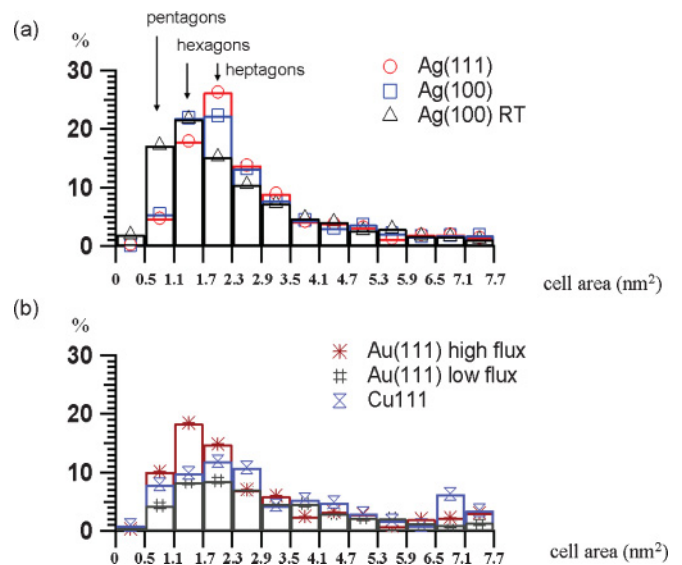


FIG. 7. (Color online) Histograms of cell areas.

Figure 7(a) gives the three histograms obtained from molecular layers grown on silver surfaces. The hexagonal, pentagonal, and heptagonal pores, i.e. the polymer units obtained after complete dehydration and covalent bonding between BDBA molecules, are the main figures. The sum of the histogram bars corresponding to hexagons, pentagons, and heptagons (centered at 1.35, 2.0 and 2.8 nm²) is indicative of the degree of polymerization, as they correspond to a local maximum formation of covalent bonds. It amounts to 58% of the surface for both Ag(111) and Ag(100), points one and two, respectively, in the (m, σ) graph. Other defects of undefined shape result from incomplete polymerization processes. The third histogram (point five) characterizes a polymer also obtained on Ag(100) but whose molecular layer was grown at low flux. This allowed the initial formation of an H-bonded phase that subsequently transitioned towards the polymer phase. The histogram is shifted towards smaller pore areas with a maximum corresponding to pentagon pores and a significant number of smaller pores (19%), meaning incomplete polymerization and explaining the relative positions of point five and point two in the graph. The three remaining histograms [Fig. 7(b)] were obtained for Au(111), Cu(111), and low flux Au(111). The sum of the histogram bars corresponding to hexagons, pentagons, and heptagons amounts to 41%, 33%, and 23% for Au(111), Cu(111), and low flux Au(111), respectively, in agreement with the respective positions of these polymers on the (m, σ) graph (points three, four, and six, Fig. 6). Compared to that for Ag(111), the histogram for Au(111) appears shifted towards small pore areas with a maximum occurrence for pentagon patterns. The hardly pronounced maxima on the Cu(111) histogram reflects the difficult polymer formation on that surface.

Finally, all statistical analyses reported here (degree of reaction advancement, MST graph method, and pore histograms) reasonably converge, revealing that polymer formation is most favored on silver surfaces and least favored on copper surfaces, the gold ones being an intermediate case. It is actually noteworthy that the same sequence was obtained by Bieri

et al. reporting on the two-dimensional polymerisation of hexa-iodo-substituted macrocycle cyclohexa-*m*-phenylene on Cu, Au, and Ag (111) surfaces.⁵³

B. The polymer growth problem

For a specific surface and a specific impinging species (for simplification with only one nucleation site), the nucleation rate expresses as:

$$n^* \propto F \exp \left[-\frac{(Ed - Es - Eg)}{kT} \right],$$

where F is the flux, Ed the desorption energy, Es the diffusion energy, and Eg the nucleation energy.¹ The nucleation energy can be taken as the activation energy in the case of an irreversible dehydration reaction occurring between BDBA molecules. Nucleation rate and subsequent growth can thus be influenced by two experimental parameters: the flux of species impinging the surface and the substrate temperature. The flux is governed by the temperature of the source, while the thermal energy of the substrate modifies the nucleation rate through the exponential term. The effect of substrate temperature on the BDBA nucleation growth process can be rationalized in terms of classical growth theory. Clearly, the diffusion energy appears to be the limiting factor in the case of the Cu(111) surface, on which the molecules appear to stick strongly and therefore diffuse very slowly at room temperature. Limited diffusion length explains the large number of nucleation centers on terraces [Fig. 2(a)]. Kinetic effects also determine the compactness of the molecular layer, which increases with substrate temperature, as shown by comparing Figs. 2(c) and 2(d). At low temperature, the weak mobility makes the reorganization of the molecular network more difficult once growing domains start to coalesce, which leaves more molecular vacancies and uncovered patches on the surface.

Molecule diffusion is easier on silver and gold surfaces where polymer nucleation occurs preferably at steps and more rarely on terraces. On these surfaces, the formation of a compact hydrogen-bonded phase indicates that diffusion is sufficient even at RT to grow an extended 2D network [Figs. 3(a) and 3(d)]. However, under heating the hydrogen-bonded phase formed on the Au(111) substrate, a major fraction of the molecules appeared to desorb rather than react and extend the polymer phase. Polymer growth was then only obtained in the vicinity of steps where molecules are more strongly anchored [Fig. 3(b)]. The same heating experiment done on Ag(111) led to a polymer phase extending from steps through terraces [Fig. 3(e)], which means that the adsorption energy of BDBA molecules should be greater on Ag(111) than on Au(111). Obviously, the molecules adsorbed on surfaces need a high mobility to react. Among the three noble metals, silver gives the best compromise between adsorption and diffusion. The adsorption energy appears to be too weak on the gold surface so that substantial molecule desorption occurs when the temperature is raised. On the contrary, molecules are more strongly adsorbed on the copper surface. This results in the formation of a large number of nucleation centers, which—associated to a small diffusion coefficient—produces unfavorable polymer growth. As evidenced by the

statistical MST approach, it is on Ag (111) and Ag(100) surfaces that the optimum experimental conditions that allow BDBA molecules to react and the polymer to form are found.

Crystal growth is a nonequilibrium process that requires the necessary time for adsorbed species to be incorporated at favorable sites so that the nearly equilibrium crystal shape can be built. Of course, this condition is fulfilled using low fluxes, and this is the usual way to grow metals and semiconductors with good crystalline quality. The striking and *a priori* counterintuitive result obtained in our case for BDBA molecules is that the best polymerization is obtained with increased molecular flux (i.e. increased source temperature). It is actually noteworthy that in the case of Cu(111) maintained at RT, polymerization occurs when the source temperature is $T_c = 110$ °C and not 90 °C [Figs. 2(a) and 2(c), respectively]. Whatever the metal nature, increasing the molecular flux enables a better polymer growth.

In fact BDBA polymer formation is a complex process that requires crossing over several steps and intermediate states before the boroxine trimer—the basis for polymer growth—can form. The theoretical reaction path from BDBA monomer to boroxine trimer was established by Sassi *et al.*⁵⁴ They calculated that the formation of a boroxine ring requires an activation energy of about 1 eV, except for the first reaction step that consists in the formation of a hydrogen-bonded dimer. Indeed, two BDBA monomers react exothermically to form the hydrogen-bonded dimer. From there to the covalent form of a dimer, an activation energy barrier should be crossed. It should be stressed that the calculations by Sassi *et al.*⁵⁴ were conducted within the frame of homogeneous nucleation, that is to say, without taking into account the effect of the surface that can modify the process and in particular the activation barriers. Nevertheless, the exothermic formation of a hydrogen-bonded dimer will always be preferred under near-equilibrium growth conditions. Therefore, monomers landing on the surface at low flux and with sufficient diffusion—which is the case for Ag and Au, but not for Cu—should preferably link by hydrogen bonds rather than by covalent bonds. Indeed, the hydrogen-bonded phase is formed experimentally in such growth conditions. Obviously, annealing the hydrogen-bonded phase induces polymer formation, provided that the molecules do not desorb, which is the case for silver but not for gold (except at step edges). The polymer obtained that way on Ag(100), however, exhibits poor structural quality [point five compared to point two in (m, σ) graph Fig. 6]. Thus, to obtain good polymer growth, it is necessary to establish the experimental conditions preventing the hydrogen-bonded phase and favoring the initial formation of dimers and boroxine trimers, precursors to more complex oligomers (see Table I). This can only be done by favoring the occurrence of multiple contacts between the molecules and the first oligomers. This condition implies a high concentration of molecular species on the surface, which is readily obtained by increasing the molecular flux. After stable nuclei have formed, the entropy stabilization becomes favorable to the extension of the polymer.⁵⁴ Of course, increasing the substrate temperature also favors the nucleation as it reduces the term $\exp(-Eg/kT)$ in the expression of n^* , and increases the diffusion of surface species.

In short, optimum polymer growth is obtained when the flux—which is source temperature dependent—and the substrate temperature—which tunes the energetic terms for adsorption, diffusion, and reaction of the molecules—can be adjusted to open some favorable window, if any, for the polymerization process.

IV. CONCLUSION

1,4-benzene-diboric acid (BDBA) molecules were vapor deposited under ultrahigh vacuum on well-oriented surfaces of noble metals, Ag(111), Ag(100), Au(111), and Cu(111), to grow a two-dimensional polymer. Testing different growth parameters (evaporation flux, substrate temperature) on all surfaces made it possible to determine the optimum experimental conditions required for the formation of a little defective polymer. It was found that a high molecular flux was necessary to perform polymerization of BDBA on all surfaces. At low flux, no specific arrangement was obtained on the copper surface, and a hydrogen-bonded supramolecular phase took place on the silver and gold surfaces. Once polymerization occurs due to a dehydration process between two BDBA molecules, it extends to grow an extended network exhibiting several kinds of defects. An ideally complete polymerization process should produce a perfect surface honeycomb network. However, besides hexagonal cells, various polygonal cells (mainly pentagons and heptagons) and incompletely reacted BDBA molecules were still observed inside the polymerized

molecular layer. Annealing the molecular layer could not significantly cure the defects, and a temperature of 450 °C had to be surpassed before the degradation of the polymer began, meaning strong covalent linking had occurred. A series of statistical analyses were performed to quantify the order hidden behind the disorder: determination of the degree of reaction advancement, pore size histograms, and minimal spanning tree approach. All data indicate that to grow a good-quality polymer Ag(111) and Ag(100) are more efficient than Au(111) and that Cu(111) is rather inefficient. Besides a high flux of molecules impinging on the surface, the polymerization process requires not only that the adsorbed molecules reside on the surface long enough, but also that they can easily diffuse on it. The surface temperature should be adjusted for each metal to allow the best surface diffusion of the adsorbed molecules and the longest residential time. Certainly these two contradictory conditions can be difficult to satisfy, as illustrated by the case of polymer growth on Cu(111). Up to now silver surfaces have demonstrated the best-quality extended two-dimensional organic polymer.

ACKNOWLEDGMENTS

This work was supported by the Agence Nationale de la Recherche under Grant ANR-2010-JCJC-1001-1. It is a great pleasure to thank Bernard Billia for drawing our attention to the minimal spanning tree approach. Mathieu Koudia and Daniel Catalin are gratefully acknowledged for experimental support.

*mathieu.abel@im2np.fr

†sylvain.clair@im2np.fr

‡Present address: CEMES - CNRS, 29 Rue J. Marvig, BP 94347, 31055 Toulouse, France.

§louis.porte@im2np.fr

¹J. V. Barth, *Annu. Rev. Phys. Chem.* **58**, 375 (2007).

²J. Elemans, S. B. Lei, and S. De Feyter, *Angew. Chem., Int. Ed.* **48**, 7298 (2009).

³A. Gourdon, *Angew. Chem., Int. Ed.* **47**, 6950 (2008).

⁴D. F. Perepichka and F. Rosei, *Science* **323**, 216 (2009).

⁵J. Sakamoto, J. van Heijst, O. Lukin, and A. D. Schlüter, *Angew. Chem., Int. Ed.* **48**, 1030 (2009).

⁶Y. Okawa and M. Aono, *Nature* **409**, 683 (2001).

⁷H. Sakaguchi, H. Matsumura, and H. Gong, *Nat. Mater.* **3**, 551 (2004).

⁸H. Sakaguchi, H. Matsumura, H. Gong, and A. M. Abouelwafa, *Science* **310**, 1002 (2005).

⁹L. Grill, M. Dyer, L. Lafferentz, M. Persson, M. V. Peters, and S. Hecht, *Nature Nanotechnology* **2**, 687 (2007).

¹⁰S. Weigelt, C. Busse, C. Bombis, M. M. Knudsen, K. V. Gothelf, T. Stunskus, C. Wöll, M. Dahlborn, B. Hammer, E. Lægsgaard, F. Besenbacher, and T. R. Linderoth, *Angew. Chem., Int. Ed.* **46**, 9227 (2007).

¹¹M. Matena, T. Riehm, M. Stöhr, T. A. Jung, and L. H. Gade, *Angew. Chem., Int. Ed.* **47**, 2414 (2008).

¹²M. Treier, N. V. Richardson, and R. Fasel, *J. Am. Chem. Soc.* **130**, 14054 (2008).

¹³M. I. Veld, P. Iavicoli, S. Haq, D. B. Amabilino, and R. Raval, *Chem. Commun.* 1536 (2008).

¹⁴S. Weigelt, C. Bombis, C. Busse, M. M. Knudsen, K. V. Gothelf, E. Lægsgaard, F. Besenbacher, and T. R. Linderoth, *Acs Nano* **2**, 651 (2008).

¹⁵S. Weigelt, C. Busse, C. Bombis, M. M. Knudsen, K. V. Gothelf, E. Lægsgaard, F. Besenbacher, and T. R. Linderoth, *Angew. Chem., Int. Ed.* **47**, 4406 (2008).

¹⁶N. A. A. Zwaneveld, R. Pawlak, M. Abel, D. Catalin, D. Gígmes, D. Bertin, and L. Porte, *J. Am. Chem. Soc.* **130**, 6678 (2008).

¹⁷M. Bieri, M. Treier, J. M. Cai, K. Ait-Mansour, P. Ruffieux, O. Groning, P. Groning, M. Kastler, R. Rieger, X. L. Feng, K. Mullen, and R. Fasel, *Chem. Commun.* **45**, 6919 (2009).

¹⁸C. Bombis, F. Ample, L. Lafferentz, H. Yu, S. Hecht, C. Joachim, and L. Grill, *Angew. Chem., Int. Ed.* **48**, 9966 (2009).

¹⁹S. Boz, M. Stöhr, U. Soydaner, and M. Mayor, *Angew. Chem., Int. Ed.* **48**, 3179 (2009).

²⁰R. Gutzler, H. Walch, G. Eder, S. Kloft, W. M. Heckl, and M. Lackinger, *Chem. Commun.* **45**, 4456 (2009).

²¹S. Jensen, H. Fruchtl, and C. J. Baddeley, *J. Am. Chem. Soc.* **131**, 16706 (2009).

²²L. Lafferentz, F. Ample, H. Yu, S. Hecht, C. Joachim, and L. Grill, *Science* **323**, 1193 (2009).

²³J. A. Lipton-Duffin, O. Ivasenko, D. F. Perepichka, and F. Rosei, *Small* **5**, 592 (2009).

²⁴C. H. Schmitz, J. Ikonov, and M. Sokolowski, *J. Phys. Chem. C* **113**, 11984 (2009).

- ²⁵M. Treier, R. Fasel, N. R. Champness, S. Argent, and N. V. Richardson, *Phys. Chem. Chem. Phys.* **11**, 1209 (2009).
- ²⁶M. O. Blunt, J. C. Russell, N. R. Champness, and P. H. Beton, *Chem. Commun.* **46**, 7157 (2010).
- ²⁷J. M. Cai, P. Ruffieux, R. Jaafar, M. Bieri, T. Braun, S. Blankenburg, M. Muoth, A. P. Seitsonen, M. Saleh, X. Feng, K. Müllen, and R. Fasel, *Nature* **466**, 470 (2010).
- ²⁸J. A. Lipton-Duffin, J. A. Miwa, M. Kondratenko, F. Cicoira, B. G. Sumpter, V. Meunier, D. F. Perepichka, and F. Rosei, *Proc. Nat. Acad. Sci. USA* **107**, 11200 (2010).
- ²⁹M. Matena, M. Stöhr, T. Riehm, J. Björk, S. Martens, M. S. Dyer, M. Persson, J. Lobo-Checa, K. Müllen, M. Enache, J. Wadepohl, J. Zegenhagen, T. A. Jung, and L. H. Gade, *Chem. Eur. J.* **16**, 2079 (2010).
- ³⁰F. Sedona, M. Di Marino, M. Sambì, T. Carofiglio, E. Lubian, M. Casarin, and E. Tondello, *Acs Nano* **4**, 5147 (2010).
- ³¹S. Jensen, J. Greenwood, H. A. Früchtl, and C. J. Baddeley, *J. Phys. Chem. C* **115**, 8630 (2011).
- ³²S. A. Krasnikov, C. M. Doyle, N. N. Sergeeva, A. B. Preobrajenski, N. A. Vinogradov, Y. N. Sergeeva, A. A. Zakharov, M. O. Senge, and A. A. Cafolla, *Nano Res.* **4**, 376 (2011).
- ³³C. H. Schmitz, J. Ikononov, and M. Sokolowski, *J. Phys. Chem. C* **115**, 7270 (2011).
- ³⁴M. Treier, C. A. Pignedoli, T. Laino, R. Rieger, K. Müllen, D. Passerone, and R. Fasel, *Nat. Chem.* **3**, 61 (2011).
- ³⁵R. Coratger, B. Calmettes, M. Abel, and L. Porte, *Surf. Sci.* **605**, 831 (2011).
- ³⁶M. Abel, S. Clair, O. Ourdjini, M. Mossoyan, and L. Porte, *J. Am. Chem. Soc.* **133**, 1203 (2011).
- ³⁷A. P. Cote, A. Benin, and N. W. Ockwig, *Science* **310**, 1166 (2005).
- ³⁸A. P. Cote, H. M. El-Kaderi, H. Furukawa, J. R. Hunt, and O. M. Yaghi, *J. Am. Chem. Soc.* **129**, 12914 (2007).
- ³⁹P. Rodriguez-Cuamatzi, G. Vargas-Díaz, T. Maris, J. D. Wuest, and H. Höpfl, *Acta Crystallogr. Sect. E.-Struct. Rep. Online* **60**, O1316 (2004).
- ⁴⁰R. Pawlak, L. Nony, F. Bocquet, V. Oison, M. Sassi, J. M. Debierre, C. Loppacher, and L. Porte, *J. Phys. Chem. C* **114**, 9290 (2010).
- ⁴¹D. Sanchez-Portal, P. Ordejón, E. Artacho, and J. M. Soler, *Int. J. Quantum Chem.* **65**, 453 (1997).
- ⁴²J. M. Soler, E. Artacho, J. D. Gale, A. García, J. Junquera, P. Ordejón, and D. Sanchez-Portal, *J. Phys. Condens. Matter* **14**, 2745 (2002).
- ⁴³The exchange-correlation energy is treated within the generalized gradient approximation using parameterization proposed by Perdew–Burke–Ernzerhof. The wave function of the valence electrons are expanded in a localized basis set consisting of a finite range of pseudo-atomic orbitals: a double-zeta basis set was used for each atom. The core electrons are treated within the frozen core approximation with norm-conserving Troullier–Martins pseudopotentials.
- ⁴⁴R. J. Gillespie, I. Bytheway, and E. A. Robinson, *Inorg. Chem.* **37**, 2811 (1998).
- ⁴⁵J. Beckmann, D. Dakternieks, A. Duthie, A. E. K. Lim, and E. R. Tiekink, *J. Organomet. Chem.* **633**, 149 (2001).
- ⁴⁶A. Hashimoto, K. Suenaga, A. Gloter, K. Urita, and S. Iijima, *Nature* **430**, 870 (2004).
- ⁴⁷J. Pantaloni and P. Cerisier, in *Cellular Structures in Instabilities*, edited by J. E. Wesfried and S. Zaleski (Springer-Verlag, Berlin, 1984).
- ⁴⁸F. Waller and C. Dussert, *Europhys. Lett.* **42**, 493 (1998).
- ⁴⁹C. Dussert, G. Rasigni, M. Rasigni, J. Palmari, and A. Llebario, *Phys. Rev. B* **34**, 3528 (1986).
- ⁵⁰B. Billia, H. Jamgotchian, and H. N. Thi, *Metall. Trans. A-Physical Metallurgy and Materials Science* **22**, 3041 (1991).
- ⁵¹N. Noel, H. Jamgotchian, and B. Billia, *J. Cryst. Growth* **181**, 117 (1997).
- ⁵²P. Cerisier, S. Rahal, and B. Billia, *Phys. Rev. E* **54**, 3508 (1996).
- ⁵³M. Bieri, M. T. Nguyen, O. Gröning, J. Cai, M. Treier, K. Aït-Mansour, P. Ruffieux, C. A. Pignedoli, D. Passerone, M. Kastler, K. Müllen, and R. Fasel, *J. Am. Chem. Soc.* **132**, 16669 (2010).
- ⁵⁴M. Sassi, V. Oison, J. M. Debierre, and S. Humbel, *Chem. Phys. Chem.* **10**, 2480 (2009).